



HAL
open science

Indurated soil nodules: A vestige of ancient agricultural practices?

Alain Giosa, Thomas Delbey, Clément Menbrivès, Kaare Rasmussen, Michelle Elliott, Christophe Petit

► **To cite this version:**

Alain Giosa, Thomas Delbey, Clément Menbrivès, Kaare Rasmussen, Michelle Elliott, et al.. Indurated soil nodules: A vestige of ancient agricultural practices?. *Geoarchaeology: An International Journal*, 2022, 37 (6), pp.870-886. 10.1002/gea.21926 . hal-03806472

HAL Id: hal-03806472

<https://hal.science/hal-03806472v1>

Submitted on 6 Dec 2024

HAL is a multi-disciplinary open access archive for the deposit and dissemination of scientific research documents, whether they are published or not. The documents may come from teaching and research institutions in France or abroad, or from public or private research centers.

L'archive ouverte pluridisciplinaire **HAL**, est destinée au dépôt et à la diffusion de documents scientifiques de niveau recherche, publiés ou non, émanant des établissements d'enseignement et de recherche français ou étrangers, des laboratoires publics ou privés.



Distributed under a Creative Commons Attribution 4.0 International License

Indurated soil nodules: A vestige of ancient agricultural practices?

Alain Giosa¹ | Thomas Delbey²  | Clément Menbrivès¹  |
Kaare L. Rasmussen³  | Michelle Elliott¹ | Christophe Petit¹

¹UMR 7041 ArScAn, Équipe Archéologies Environnementales, University Paris 1 Panthéon-Sorbonne, Paris, France

²Cranfield Forensic Institute, Defence Academy of the United Kingdom, Cranfield University, Shrivenham, UK

³Department of Physics, Chemistry and Pharmacy, Cultural Heritage and Archaeometric Research Team, University of Southern Denmark, Odense M, Denmark

Correspondence

Thomas Delbey, Cranfield Forensic Institute, Defence Academy of the United Kingdom, Cranfield University, Shrivenham SN6 8LA, UK.

Email: Thomas.Delbey@cranfield.ac.uk

Abstract

The identification of controlled fires in ancient agricultural systems is important for understanding how past societies managed the landscape. Although the use of fire in agriculture is documented in recent historical records, and combustion markers can persist in soils over a long time scale, this is a complex issue because combustion traits in general are ubiquitous. Archaeopedological surveys undertaken in an ancient forest in Burgundy (France) have led to the recovery of several red indurated nodules scattered in the soils. Gallo-Roman housing structures and parcels were recognized using light detection and ranging mapping, stimulating questions about the understanding of the nature of these nodules. Elemental and structural analyses by X-ray fluorescence and X-ray diffraction (XRD) confirmed the local origin of these features by comparing their composition with on-site sediments, and thermoluminescence dating placed the samples in the Medieval period. The results cast light on the nature of the nodules and how they can be related to controlled fires used in agricultural practices. Even though questions remain about which processes lead to the formation of the nodules, the firing temperature estimated via XRD analysis seems to be in agreement with that used in the “paring-and-burning” technique. The present study provides new information about medieval agriculture practices from the 10th to the 12th centuries CE and shows how past societies managed the opening and maintenance of agricultural fields using natural resources and “archaeological” remains from the antique period.

KEYWORDS

agricultural practices, archaeopedology, indurated soil nodules

Scientific editing by Sarah Sherwood.

Alain Giosa and Thomas Delbey should be considered as joint first author.

This is an open access article under the terms of the Creative Commons Attribution License, which permits use, distribution and reproduction in any medium, provided the original work is properly cited.

© 2022 The Authors. *Geoarchaeology* published by Wiley Periodicals LLC.

1 | INTRODUCTION

Indurated nodules are occasionally discovered during archaeological, pedological, or geological surveys. This type of material, nowadays known from a wide range of environments, can measure up to 5 cm in diameter and shows a wide variety of shapes, structures, and colors. Depending on the context where they are found and physical characteristics, indurated nodules can generally be associated with two different formation processes, namely, accumulation of Fe and Mn, or exposure to fire, both of which cause the sediment to aggregate. However, the wide variability of their characteristics and the lack of systematic analysis focused on the nodules discovered in archaeological investigations often result in confusion when it comes to the interpretation of such finds (Aldeias, 2017). The hypothesis of exposure to fire is usually put forward in archaeological settlement contexts, supported by the presence of a reddened layer and the detection of charcoal and other charred materials found along with the nodules (Macphail et al., 1990; Macphail & Goldberg, 1990). However, determining if a fire event was natural or anthropogenic is still a challenge for archaeologists.

Fire is considered as an ancient and important factor in landscape evolution. Attempts to identify the first controlled fire during the Pleistocene have resulted in a vigorous debate among specialists (Brain & Sillent, 1988; Canti & Linford, 2000; Roebroeks & Villa, 2011; Weiner, 1998). The discovery of burnt ecofacts, together with archaeological structures or artifacts related to agricultural activities, has been considered a key element for the identification of agricultural fire practices, also supported by modern ethnographic observations in Asia, South America, and Africa (Bentsen, 2013; Ketterings et al., 2000). However, there remain many uncertainties about the impact and the extent of this practice on agricultural systems of past societies, namely, due to the problems of identification of burnt remains. (Aldeias, 2017; Canti & Linford, 2000; Guiblais-Starck et al., 2020; Ponomarenko et al., 2019).

From a practical perspective, many questions remain about how fire impacts the topsoil over the short and long term. The temperature of the fire and its residence time (time occupied by the flame front on a surface area) are key parameters to understanding the mineralogical and structural changes in the soil. Experimental archaeology provides some insightful data about the short-term effects of fire on soils, but the limited numbers of such studies fail to completely answer questions about the nature of past fire events.

In the forest of Châtillon (Burgundy, France), an archaeological surface survey and light detection and ranging (LiDAR) mapping have yielded the identification of a network of roads and agricultural parcels that are linked to different types of archaeological structures representing a discontinuous occupation from the La Tène A period (c. 450 BC) until modern times (Chevigny et al., 2018; Goguey et al., 2018; Pautrat & Goguey, 2004). The archaeopedological field survey has revealed red, brown, and black indurated nodules, millimetric to centimetric, scattered in the profiles of various pedological pits below the organic horizon. Although the soil laboratory preparation

indicates that these markers are tenuous, they are recurrent, since about 60% of the sampled soils show such nodules. Since the origin of these nodules is unclear, a series of analyses were performed to identify their nature. Were the indurated nodules naturally occurring, resulting either from pedological processes or wildfires, or did they result from anthropic activities related either to fire in connection with agricultural practices or manuring (garbage spreading originating from houses)? If their formation was related to human activities, their dating would provide important information about the history of ancient agricultural techniques in use during this time period.

This study is innovative in three aspects. First, the use of LiDAR technology provides a powerful tool to identify the agricultural parcels where the samples were collected (Georges-Leroy, 2009; Georges-Leroy et al., 2011). Second, a novel analytical strategy, based on elemental and mineralogical characterization provided by X-ray spectrometry, X-ray diffraction (XRD), and petrographic microscopy, was applied to characterize the indurated nodules and their surrounding sediment. Finally, for the first time, to the best of our knowledge, thermoluminescence dating provides absolute dates of indurated nodules in archaeological contexts.

2 | ON THE ORIGIN OF INDURATED NODULES IN SOILS

Three different theories for the formation of the nodules have been put forward in the literature. First, nodules could be related to Fe–Mn concretions produced by the pedogenetic process and mistaken for combustion residues. The mobilization, transfer, and accumulation of Mn and Fe ions in soils would, in this case, be responsible for the formation of the Mn–Fe rich nodules (Šegvić et al., 2018; Sun et al., 2018; Tan et al., 2006). The availability of these ions in soils is largely determined by the alternation of redox potential in the soil system, which is again driven by the topsoil water regimes, microbial activities, and temperature changes induced by seasonal climate variations (Fitzpatrick, 1988; Vepraskas, 2000). The mobility of the Mn–Fe ions is increased during the wet seasons in anaerobic conditions when Fe³⁺ and Mn^{3+/4+} are reduced to Fe²⁺ and Mn²⁺. During the dry seasons, reoxidation in aerobic conditions decreases their solubility, leading to precipitation (Gasparatos, 2011). The Mn–Fe accumulation can emerge in different forms such as spherical, oval, or irregular-shaped nodules, with a wide range of colors in brown–orange–yellow hues (Latrille et al., 2001; Šegvić et al., 2018). While the shape of the nodule can vary according to the type of soil and depth in the soil profile (Phillippe et al., 1972), the hue seems to depend mainly on the concentration of Mn (Rabenhorst & Parikh, 2000). Some concretions show a concentric internal structure organized around a nucleus, while some others do not (Gasparatos, 2011). Occasionally, the Mn–Fe accumulation can also appear as a simple partial or complete coating of soil aggregates, thus modifying their color, texture, and stability (Baize & Jabiol, 1995; Stoops et al., 2018; Xue et al., 2019).

Second, a hypothesis has been put forward related to a direct impact of fire on soil. Various types of fire events can affect soil color,

texture, and mineralogy, and also lead to the formation of burnt soil nodules. In a forest environment, wildfires usually occur when an abundance of dry fuel is available (Certini, 2005). However, the ignition processes of wildfires, their severity (temperature and residence time), and their impact on soil and vegetation depend on atmospheric and ecosystem conditions, both on a local and on a temporal scale (Neary et al., 1999; Zavala et al., 2014). Controlled fires used for agricultural purposes are mainly divided into two types (Sigaut, 1975): the "paring-and-burning" technique (*écobuage* in French), which consists of removing the surface layer of a field, burning it (usually by forming oven-like combustion structures made of the removed sods), and then spreading the residues to improve the chemical properties of soil for agriculture (Nzila, 1992). The second type is the "slash-and-burn" technique (*éssartage* in French), which is related to the clearance of land that has not been cultivated for a long time, if ever. This technique generally consists of felling the trees, chopping the wood, and gathering it with the remains of the other vegetation present, and then burning it all to clear the area. Depending on the chrono-geographical context, several variations of these two methods have been observed (Jobbé Duval et al., 2007; Portères, 1972; Sigaut, 1975; Steensberg, 1993). The effects of fire on soil exposed to wildfires or controlled fires are variable according to the severity of the fire, the pedological context (texture, humidity, organic matter content), the available fuel (nature, humidity, amount), and the postfire conditions (Certini, 2005; Mataix-Solera et al., 2011). The renewal of organic matter provides better availability of nutrients and improves cation-exchange capacity (Johnson & Curtis, 2001). It will also lead to a short-term increase in pH due to the release of alkaline cations. Firing also affects the biological and physical properties of soils such as water repellence, aggregate stability, and bulk density (Certini, 2005; Thomaz, 2017). Soil granulometry, and the type and amounts of cementing substances (organic substances, Fe–Al oxides, or calcium carbonate) are key variables that can either increase or decrease these parameters depending on the severity of the fire (Mataix-Solera et al., 2011; Thomaz, 2021). Mineralogical transformation in soil is a complex process involving numerous factors. However, the severity of the fire, the firing atmosphere (reducing or oxidizing), and the soil chemistry are usually considered to be the most important parameters. The first changes usually occur at around 300°C with the dehydroxylation of goethite and its transformation into maghemite or proto-hematite (Gualtieri & Venturelli, 1999), followed by the decomposition of kaolinite and chlorite between 500°C and 600°C (Jordán et al., 1999; Steudel et al., 2016). The formation of Fe oxide is responsible for the reddening of the soil after a fire. This depends on the availability of Fe, but experiments undertaken by Canti and Linford (2000) and Ketterings et al. (2000) have shown a complex situation, where the fire severity, the soil humidity, crystal size, and the presence of ashes have a strong influence on soil rubefaction (Röpke & Dietl, 2017). Finally, in the case of natural fires, it must be considered that the physical changes are usually highly variable in space, depending on the initial distribution and properties of the fuels (mosaic), and that in most cases, the temperature decreases rapidly in the first few centimeters below the ground surface (Parson et al., 2010; Scott et al., 2014).

The third possibility is related to the mistaken identity between indurated nodules and fragments of ceramics, bricks, roof tiles, or burnt earth building materials (e.g., daub). Indeed, the discovery of eroded sherds has been recorded in ancient fields and interpreted as markers of agricultural spreading in association with fertilizer materials from domestic contexts used for soil amendments (Poirier & Laüt, 2013; Poirier & Nuninger, 2012).

3 | THE STUDY AREA

The forest of Châtillon is located on a Jurassic limestone plateau delimited to the west by the Ource and Digeanne valleys, and to the east by the Seine and Brevon valleys. This karstic plateau is located near the south-eastern limit of the Parisian Basin (Figure 1). The history of the forest goes back to the end of the 14th century CE, when the area was part of the Burgundy ducal property dedicated to wood and charcoal production. Later, the forest then became a royal and a domanial property owned by the state (Beck & Beck, 2007). The continuity was related to the forest exploitation providing fuel for the intensive metallurgic activities that took place in the Châtillonnais area from the 16th to the 19th centuries (Benoît & Rignault, 1984–1986; Goguy et al., 2010). The forest altitude varies between c. 300 m above sea level to the north and c. 400 m in the south. The mean annual rainfall is 810 mm, and the mean annual temperature is 10°C. The forest of the study area generates a special microclimate: even though the altitude is low, phytological indicators are characteristic of a middle-altitude climate with the presence of *Vaccinium myrtillus*, *Gentiana lutea*, and *Ligularia siberica* (Nicloux, 1986). The study area contains two types of soils strongly tied to the nature of the limestone bedrock from the Bathonian period (166–168 My). A thin layer of silty clay calcisol with ferralic properties overlies the hard Comblanchien limestone, while a thin layer of rendzic soil and calcisol overlies the soft oolitic limestone. The origin of these silty clay particles seems to be related to wind deposition from a Callovian period formation (166–163 My) located near to the north. The soils of these karstic plateaus are usually porous and therefore not affected by water table fluctuations. However, specific pedologic horizons show a reddish color, indicating the presence of Fe-rich oolites resulting from karstic alteration (Baize, 2012; Leneuf & Puisségur, 1976). The territory occupied by the forest and its surroundings shows multiple indicators of ancient human activities. Several burial mounds (tumulus) from the La Tène A (450–380 BCE) and La Tène B (380–250 BCE) periods are known in this area (Chaume, 1999; Cruz, 2012; Goguy et al., 2018). The transition to the La Tène C period (250–150 BC) is marked by the use of a new inhumation practice in funerary pits usually located in a quadrangular enclosure, as well as the development of new housing structures and small towns (Chevrier, 2011). From the La Tène C (250–150 BCE) and Gallo-Roman periods, two sanctuaries and about 80 housing structures have been detected and some of them have been excavated in this area along with many archaeological tools related to agricultural activities such as scythes, sickles, and plough-share. From the 6th century CE, the historical archives from the Côte

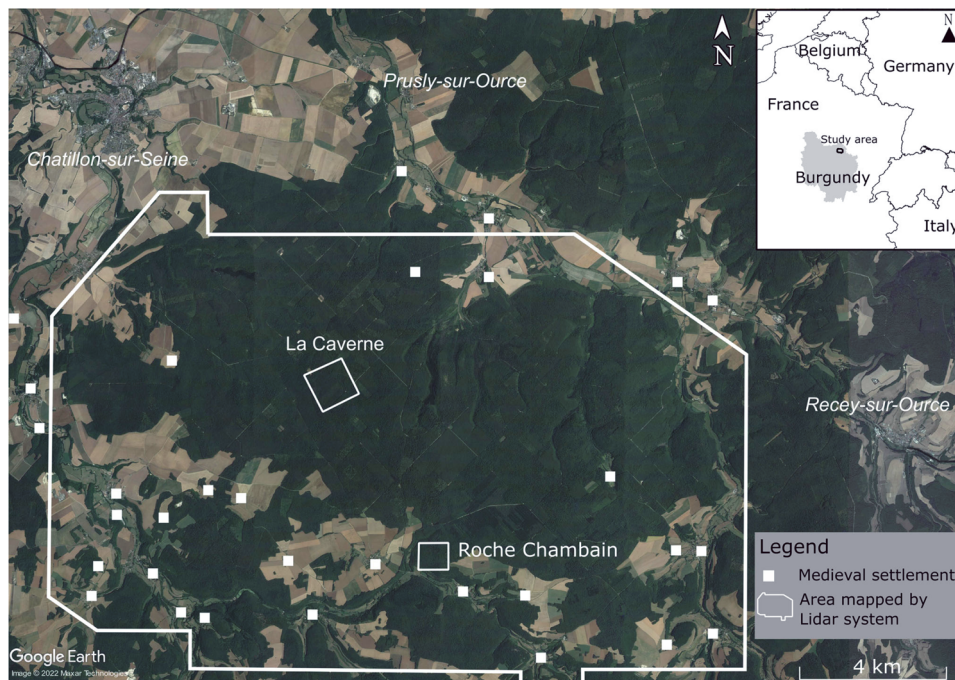


FIGURE 1 Location of the study site in the forest of Châtillon, Burgundy. The background satellite picture was downloaded on Google Earth Pro. The names of the modern towns are in italic. [Color figure can be viewed at [wileyonlinelibrary.com](https://onlinelibrary.wiley.com/doi/10.1002/gea.21926)]

d'Or department mention settlements mainly concentrated in villages around the forest, and sarcophagi from the Merovingian period were also discovered (Provost, 2009a, 2009b; Roserot, 1924). By the end of the 12th century CE, a Commandery of the Knights Templars was built and the abbey of Val-des-Choues was founded by the Cistercian order. From medieval and recent periods, remains of burning places and huts used by charcoal production workers were discovered (Giosa, 2020; Goguy et al., 2010).

Two specific sites were selected within the study area: “La Roche Chambain” and “La Caverne” (Figure 1). Archaeological and LiDAR surveys led to the identification of a network of roads and agricultural parcels, each about 150 km². The excavations showed an occupation starting from the La Tène A period (close to 450 BCE). However, most of the archaeological remains are dated to the La Tène D (150–30 BCE) and Gallo-Roman (1st century BC to end of the 5th century CE) periods. A few structures related to forestry activities from modern time have also been discovered (Giosa, 2020; Goguy et al., 2018, 2014). Evidence of Early Roman Empire settlements with parcel demarcations was found on both sites, as well as nondated coal production spots, and residues of silviculture management. The parcels and their extensions generally form geometrically homogeneous clusters. They are dated using the chronology of the settlements with which they are connected. Even though no extensive excavation has been undertaken at the two sites, the metallic artifacts (mainly fibulae and coins) and the ceramics (sherds of amphora and sigillata) collected during surface surveys are dated from the 1st century BC to the 2nd century CE (Giosa, 2020; Goguy et al., 2010). However, the superposition of parcel limits detected through LiDAR mapping hints at multiple phases of occupation of the sites.

The site of “La Roche Chambain” is about 42 ha (0.42 km²). The settlement consists of small structures built in dry stone. The main building is located at the top of a slope, dominating the radial cellular system. The limits of these parcels consist of low walls or banks that are still visible. The site of “La Caverne” is delimited by two shallow dry valleys located on the edge of the plateau on about 125 ha (1.25 km²). This area is marked by a radial cellular grid with a small Gallo-Roman villa. The building is part of an enclosure measuring of about 1.5 ha. The architecture of the villa is inspired by Mediterranean culture with the presence of painted plaster and a Roman-type arch. The limits of the parcels are mainly determined by the presence of small banks visible on the LiDAR maps (Giosa, 2020; Goguy et al., 2018).

The soils observed in the archaeological parcels on the two sites were very thin, rarely exceeding 0.3 m in depth (Figure 2). Two main types of soil were identified: the first one is a rendzic soil showing a single calcareous A horizon on the top of the limestone bedrock. The second one is a calcisol showing a Bw horizon formed of decalcification clay between a decalcified A horizon and the bedrock.

4 | MATERIALS AND METHODS

4.1 | Field methods and sampling strategy

At the “La Roche Chambain” site, the good visibility of the limits of the parcel permitted a systematic sampling strategy where five pedological pits were excavated within each parcel; a total of 154 pedological pits and all horizons were sampled. The pits yielded a total of 233 soil samples, each c. 0.25 L. At the “La Caverne” site, the

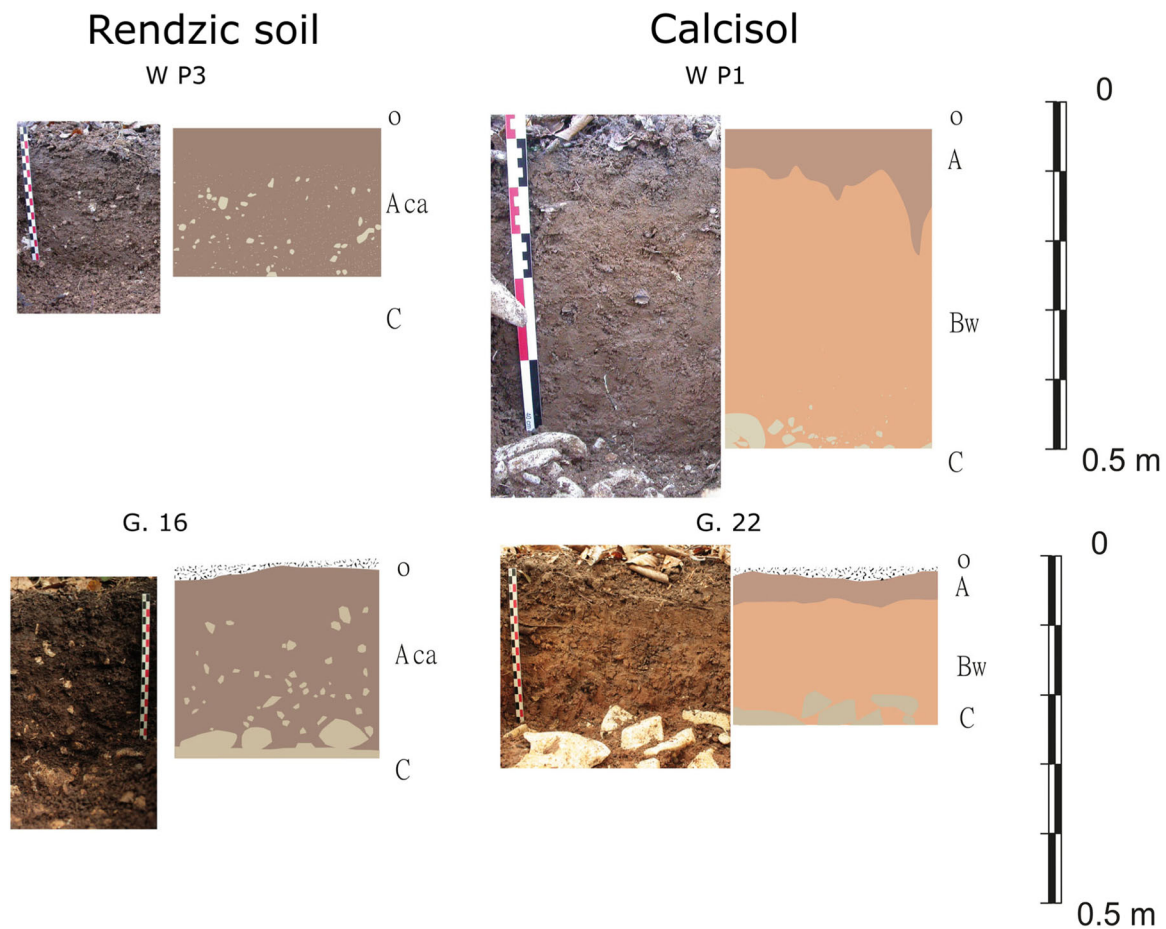


FIGURE 2 Typical soil profiles from Roche-Chambain and La Caverne sites. O—Litter. Aca—Calcareous A horizon: silty clay, brown, carbonated, granular structure, many gravel unsorted, very strong biological activity. A—A horizon: silty clay, reddish-brown, decarbonated, granular to angular structure, very strong biological activity. Bw—Decalcification clay B horizon: clay, reddish, decarbonated, angular to prismatic structure, medium biological activity. C—Top of the calcareous bedrock: Rounded boulders of limestone. [Color figure can be viewed at wileyonlinelibrary.com]

low visibility of the parcel limits led to the use of a more classic systematic sampling protocol based on a grid superposed onto the map. At this site, 234 pedological pits were excavated. Each pit was documented, and a sample was collected from the first horizon below the litter. If the A horizon was thinner than 5 cm, the samples were taken in the Bw horizon. The descriptions of the pits allowed the identification of the horizons. In those pits showing typical sequences, each horizon was sampled. The same regular grid-based protocol was then applied to three subareas to increase the spatial resolution. The 0.25 L collected soil samples were dry-sieved manually on a 4, 2, 1, 0.5, and 0.2 mm mesh column, and ground in a porcelain mortar. The material was sorted according to their type (nodules, ceramic, charcoal, etc.), counted, and weighed. Charcoal and indurated nodules were recorded and analyzed according to the protocol established by Py (2006). Indurated nodules were found in about 60% of the pits without preferential distribution and independent of any artifact concentration. The mean concentration of these nodules in the sampled soils is about 6.6 g L^{-1} , ranging from 0 to 25 g L^{-1} .

To identify and characterize the indurated soil nodules, nodules and the surrounding soil samples were collected from 15 pedological pits (Figure 3). The pits were selected in order to provide samples from the different archaeological contexts identified on the two sites. They must also contain nodules big enough to allow their analysis following the protocols, as detailed below. All pits were located inside the parcels. As the pedological study was focused on the agricultural practices of premodern periods, only the red and yellow nodules were selected. Indeed, the black nodules could be suspected to originate from modern charcoal production. To compare the composition of the nodules with the ceramics, 10 sherds were selected during the sieving process of the soil samples or during surface surveys.

All the samples were analyzed by X-ray fluorescence (XRF), and the elemental compositions of the indurated soil nodules were compared to those of the surrounding sediments and the ceramics. XRD was performed on 15 pairs of nodules and the surrounding sediment collected on the two sites to compare their mineralogical composition. In addition, nine aliquots of each of the surrounding soil samples were fired to 500°C to compare their mineralogical composition with that of

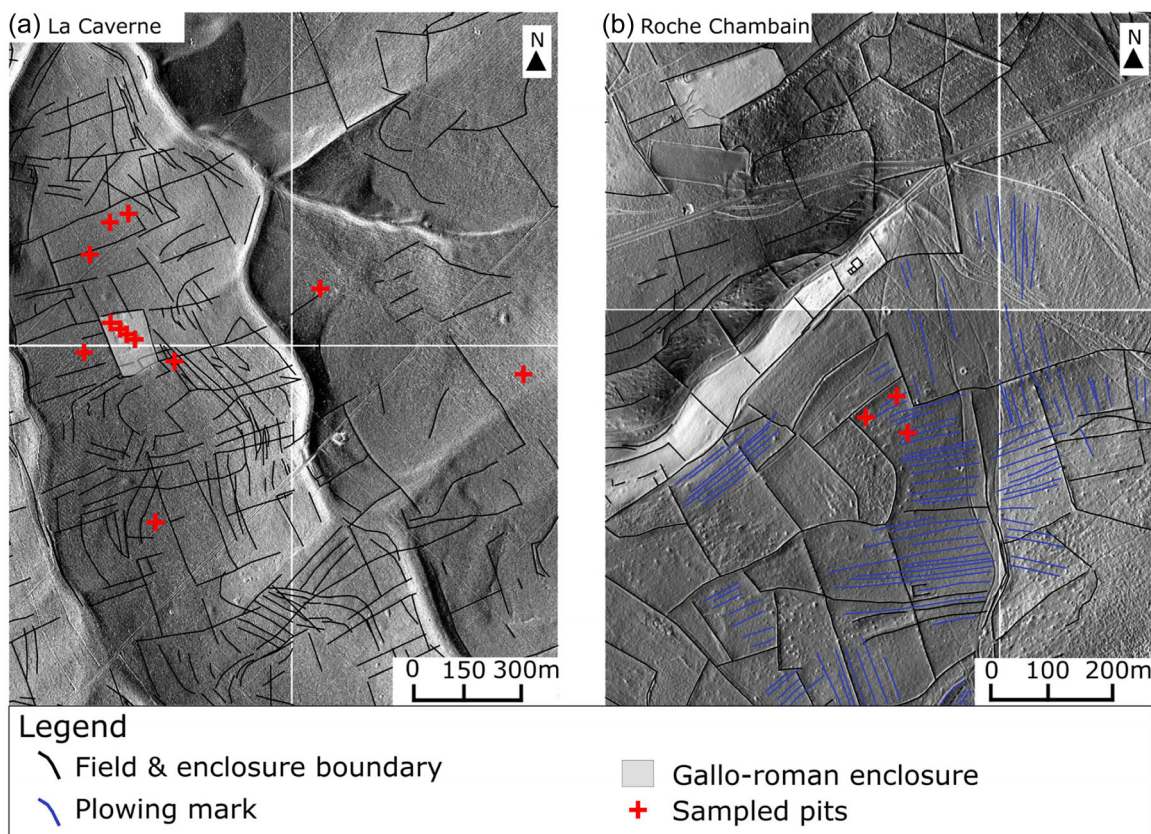


FIGURE 3 Location of the samples on the LiDAR map of the area. The drawn lines correspond to the interpretation of the micro topographical feature observed. [Color figure can be viewed at wileyonlinelibrary.com]

the nodules. These analyses helped to estimate the firing temperature of the nodules. Thermoluminescence dating was performed on 10 indurated nodules and three charcoal fragments were dated with radiocarbon. Magnetic susceptibility and colorimetry measurements were also undertaken on the nodule to evaluate the effects of the firing on the mineralogy of the samples. These results are not presented here as they are part of an ongoing project. Moreover, the use of XRD to assess mineralogical changes also provided useful information about the origin and the composition of the nodules.

4.2 | Laboratory analyses

4.2.1 | XRF analysis

The XRF analysis was performed using a benchtop ED-XRF Rigaku QC + Quantex spectrometer equipped with a silicate drift detector, a 6-position automatic sample changer, and a He purge with a flow of 0.2L min^{-1} . The spectrometer was operated at a voltage of 50 kV and at a current of $169\ \mu\text{A}$. Automatic primary filters were used to improve the detection of mid-Z and high-Z elements. The procedure for sample preparation was as follows: (1) the samples were calcined at 950°C for 6 h; (2) the samples were crushed manually in an agate mortar and the powder was sieved keeping the fraction below $300\ \mu\text{m}$; and

(3) $400 \pm 5\ \text{mg}$ of the sample powder was weighed. The quantification was performed using the international standards materials NIST-2711a Montana soil II and NIST-98b Plastic clay, both measured under the exact same conditions and with the same weights as the samples.

4.2.2 | XRD analysis

The XRD analysis was performed using a Rigaku Miniflex 600 diffractometer with Cu K α radiation as the source ($\lambda = 1.54\ \text{\AA}$) and a scintillation counter (NaI) detector. The X-ray generator was set to an acceleration voltage of 40 kV and the filament emission was set to 15 mA. The samples were analyzed in powder mode. All measurements were performed with a 2θ angle step size of 0.02° and a counting time of 10 s per step in a range from 5° to $90^\circ\ 2\theta$. The qualitative analysis was performed using *Highscore Plus* software linked to the ICDD PDF-2 database. The semi-quantitative results were determined using the reference intensity ratio (RIR) method.

4.2.3 | Petrographic analysis

The petrographic analysis was performed on a Nikon Eclipse LV100N petrographic microscope equipped with a Nikon DS-Fi2 camera. For

the quantitative evaluation, JMicroVision software (Roduit, 2007) was used. The samples were embedded under vacuum with epoxy resin before being mounted on glass slides and polished.

4.2.4 | Thermoluminescence dating

Thermoluminescence (TL) measurements were performed on a DA-12 TL-reader manufactured by Risø National Laboratory in Denmark with the 100–300 μm granulometric fraction of sieved grains using a Single Aliquot Regeneration method adapted from Hong et al. (2006), taking the average of four subsamples. Samples were treated with concentrated HCl and concentrated H_2O_2 to dissolve any carbonates and to remove any organic matter, respectively. The calculation of the date required determination of the dose received from the environment. This was assumed to originate from three sources: (1) the internal source from the four radioactive isotopes present in the samples, K40, Th232, U235, and U238; (2) the external source from the same four radioactive isotopes in the surrounding soil; and (3) the cosmic flux. The radioactive isotopes from the samples and the surrounding sediment were measured using laser ablation inductively coupled plasma mass spectrometry (LA-ICP-MS) (for Si, Th, and U) and XRF (for Si and K). The cosmic flux was estimated from the geographical position of the site, its altitude above sea level, the depth of finding, and the density of the overlying sediment. The calculation was performed using the "Luminescence" package on R software (Kreutzer et al., 2012). The procedure required the input of several parameters: (1) the self-shielding was calculated using a measured average density of $1.8 \pm 0.3 \text{ g cm}^{-3}$, (2) the grain diameter after sieving was assumed to be $200 \pm 100 \mu\text{m}$, (3) the alpha efficiency was assumed to be 0.10 ± 0.02 according to Olley et al. (1998), and (4) the sediment water content was calculated according to: water (%) by mass = $([\text{wet mass} - \text{dry mass}]/\text{dry mass}) \times 100$ (Durcan et al., 2015). The measurements of the water content were performed on the day of the sampling. No hydrogen fluoride etching was performed; thus, the alpha particle dose was included in the annual dose rate calculation (Liritzis et al., 2008). These parameters were computed and processed using AGE software (Grün, 2009), providing the dose rates and the TL ages.

To calculate the contribution of the natural radionuclides U and Th, LA was performed using a CETAC LXS-213 G2 equipped with a NdYAG laser operating at the fifth harmonic at a wavelength of 213 nm. A 25 μm circular aperture was used. The shot frequency was 20 Hz. A line scan was performed with a scan speed of $20 \mu\text{m s}^{-1}$ and was c. 300 s long following a 10 s gas blank. The helium flow was 600 ml min^{-1} . The laser operations were controlled using DigiLaz G2 software provided by CETAC. ICP-MS analyses were carried out using a Bruker Aurora M90 equipped with a frequency matching RF-generator. The basic parameters were as follows: radiofrequency power 1.30 kW; plasma argon gas flow rate 16.5 L min^{-1} ; auxiliary gas flow rate 1.65 L min^{-1} ; and sheath gas flow rate 0.18 L min^{-1} . The following isotopes were measured, all without skimmer gas: Si29, Th232, and U238. No interference corrections were applied to the selected isotopes. The analysis mode used was peak hopping with three points per peak, and the dwell time

was 10 ms on Si29 and 100 ms on Th232 and U238. The data were averaged using 5-point moving averages. The quantification was performed using a method similar to that of (Golitzko & Terrell, 2012). An in-house ceramic standard was run before and after batches of three samples to monitor the stability of the beam. The concentrations of U and Th were calculated by comparison of the U/Si and Th/Si experimental ratios to the U/Si and Th/Si standard material ratios. A relative error of ca. 10% is estimated from these measurements mostly due to the mineral heterogeneity of the samples.

4.2.5 | Radiocarbon dating

Radiocarbon analyses were performed by the Poznań Radiocarbon Laboratory. Calibrated dates were obtained using the Groningen Calib 810 program using the IntCal20 atmospheric curve data set (Reimer et al., 2020).

5 | RESULTS

5.1 | Micro- and macroscopic description of the nodules

The nodules were in a range of shapes from subspherical to subangular (Figure 4). Because of the sieving protocol used in this study, the nodules collected measured between 0.1 and 6 cm in diameter. Smaller nodules ($<0.1 \text{ cm}$) were observed under the microscope in the sieve residues, but they were not sampled. The selected nodule weights were between 0.5 and 10.0. Usually, small nodules ($<5 \text{ mm}$) were more abundant than the bigger ones, and their shapes were more spherical. According to the Munsell color chart, most of the nodules had a red (10R) or red-yellow hue (2.5YR/5YR/7.5YR).

Microscopic examination of thin sections made from the nodules (Figure 5) showed a strong similarity between the samples. In cross-polarized light (XPL), the matrix was red-brown, with medium to low anisotropy. The abundant porosity showed various shapes, but polyconcave vughs and channels were the most frequent. These



FIGURE 4 Macroscopic photographs of the sample nodules analyzed in this study. [Color figure can be viewed at wileyonlinelibrary.com]

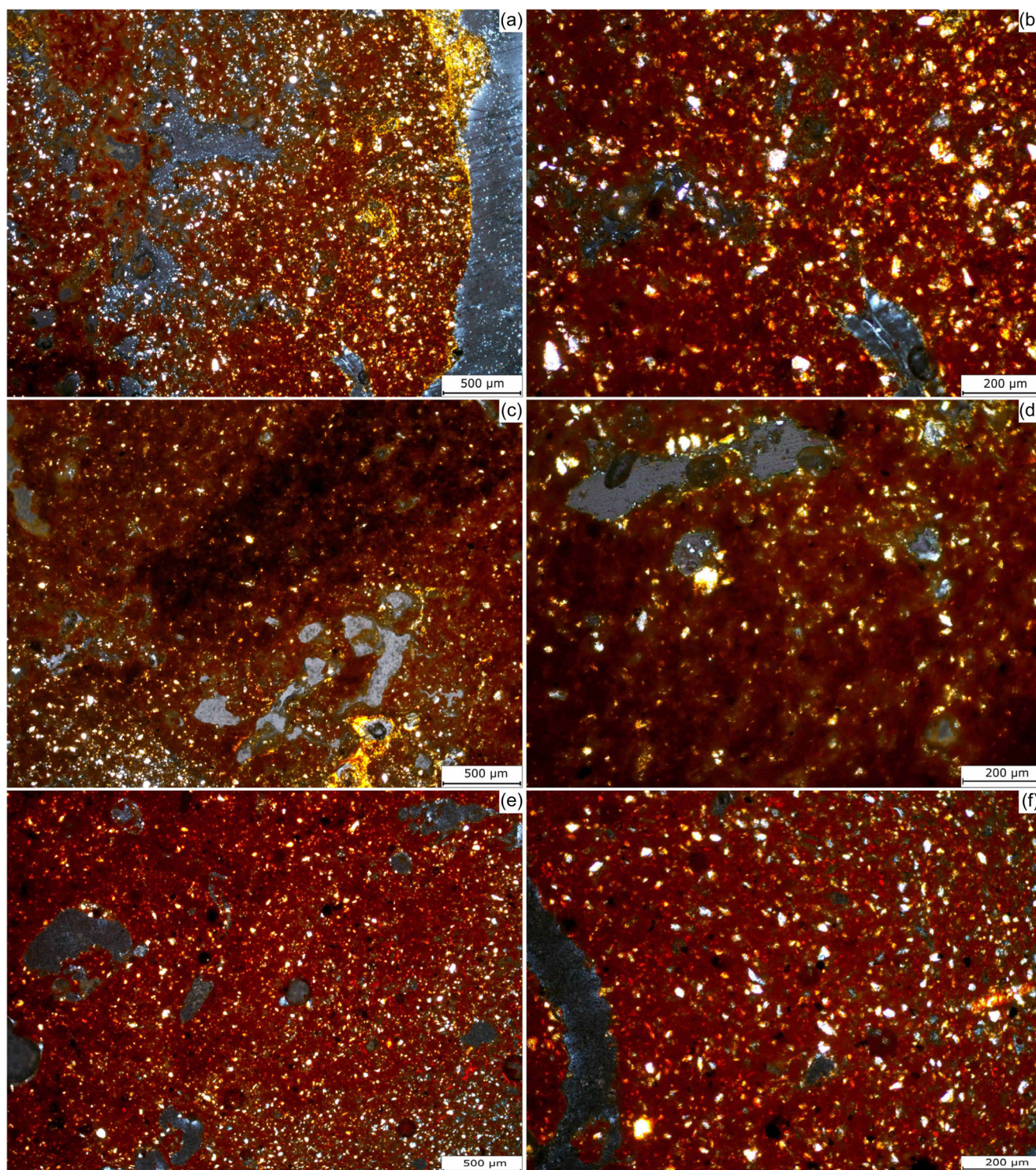


FIGURE 5 Photomicrographs from thin sections (XPL). (a, b) Sample NOD-244; (c, d) sample NOD-E14; and (e, f) soil aggregate fired to 500°C in the laboratory. XPL, cross-polarized light. [Color figure can be viewed at [wileyonlinelibrary.com](https://onlinelibrary.wiley.com/doi/10.1002/gea.21926)]

might be linked to the relatively low density of the nodules or to biological activity. Quartz was the most abundant mineral. Occasionally, micritic carbonate crystals, fine muscovite grains, and small opaque iron oxides were seen in the thin sections. The most abundant grain sizes were silt (<63 μm) and very fine sand (between 63 and 125 μm) with a mean diameter between 40 and 60 μm. The

grain size distribution was quite homogeneous, and only one modality seemed to be present. The dark spans that can be seen on microphotographs of samples NOD-244 and NOD-E14 are probably related to the remains of organic matters or charcoal. Hypocoating was not detected, suggesting an absence, or at least a low influence, of hydromorphism. The comparison between the nodules and the

experimental nodules made from fired aggregates found on the site (Figure 4) showed a stunning similarity in the structure, texture, and mineralogical composition. The same minerals were seen, and their sizes were also quite similar. The main difference was the absence of a dark span and a redder matrix of the experimental samples. This is likely caused by the absence of organic matter during the experimental firing in the electric oven, which also created a more oxidizing atmosphere, which is optimal for transforming free Fe into red iron oxide, hematite.

5.2 | XRF results

Seventeen elements were quantified by the XRF analysis: Mg, Al, Si, K, Ca, Ti, V, Cr, Mn, Fe, Co, Ni, Cu, Zn, Rb, Sr, and Ba (XRF data are

available in Supporting Information Material 1). Table 1 summarizes the classical statistical indexes and the results of a Conover-Iman's test pairwise comparison performed after a Kruskal-Wallis analysis of variance.

The relative standard deviation showed a trend of higher variability in the ceramics than in the indurated nodules and the soil samples. The distributions of Si, Ca, Mn, and Cr showed no significant differences between the indurated nodules and the soil samples according to Conover-Iman's test, whereas significant differences were seen between the pairs of soil samples/ceramics and nodules/ceramics. Conover-Iman's test showed no difference between the three types of sample for K, V, Fe, Co, Ni, Cu, and Ba. Significant differences between the three types of samples were detected for Al and Ti. The distribution of Zn was the only element that showed a significant difference between the soil samples and the indurated nodules.

TABLE 1 Minimum, maximum, mean, and RSD values for the three types of samples: indurated nodules, soil samples, and ceramics

| | Al (%) | Si (%) | K (%) | Ca (%) | Ti (%) | Mn (%) | Fe (%) | Mg (%) | |
|---|---------|----------|----------|----------|----------|----------|----------|----------|----------|
| Nod-Min. | 7.37 | 30.27 | 1.18 | 0.3 | 0.57 | 0.05 | 3.02 | 0.81 | |
| Nod-Max. | 10.21 | 37.96 | 1.81 | 3.08 | 0.74 | 0.12 | 5.43 | 1.08 | |
| Nod-Mean | 8.55 | 33.73 | 1.51 | 0.89 | 0.66 | 0.09 | 4.52 | 0.96 | |
| Nod-RSD | 0.1 | 0.05 | 0.09 | 0.76 | 0.06 | 0.2 | 0.12 | 0.06 | |
| Soil-Min. | 6.9 | 31.34 | 1.3 | 0.48 | 0.58 | 0.07 | 3.65 | 0.92 | |
| Soil-Max. | 8.93 | 37.13 | 1.85 | 3.33 | 0.66 | 0.14 | 5.04 | 1.09 | |
| Soil-Mean | 7.53 | 34.17 | 1.54 | 1.08 | 0.61 | 0.09 | 4.19 | 1 | |
| Soil-RSD | 0.07 | 0.05 | 0.1 | 0.74 | 0.03 | 0.21 | 0.1 | 0.05 | |
| Cer-Min. | 10.27 | 23.79 | 0.56 | 0.82 | 0.66 | 0.02 | 1.6 | 0.91 | |
| Cer-Max. | 14.53 | 33.75 | 3.54 | 9.83 | 1.02 | 0.15 | 5.44 | 1.15 | |
| Cer-Mean | 12.65 | 28.78 | 1.52 | 2.14 | 0.81 | 0.05 | 3.89 | 1 | |
| Cer-RSD | 0.11 | 0.11 | 0.6 | 1.21 | 0.13 | 0.67 | 0.35 | 0.08 | |
| Conover-Iman's test <i>p</i> value | | | | | | | | | |
| Soil—Cer | <0.0001 | <0.0001 | 0.352 | 0.021 | <0.0001 | 0 | 0.597 | 0.694 | |
| Nod—Soil | <0.0001 | 0.423 | 0.795 | 0.477 | <0.0001 | 0.342 | 0.075 | 0.096 | |
| Nod—Cer | <0.0001 | 0 | 0.483 | 0.004 | <0.0001 | 0.002 | 0.277 | 0.264 | |
| | V (ppm) | Cr (ppm) | Ni (ppm) | Cu (ppm) | Zn (ppm) | Rb (ppm) | Sr (ppm) | Co (ppm) | Ba (ppm) |
| Nod-Min. | 62.55 | 47.52 | 15.38 | 76.99 | 104.65 | 50.27 | 30.58 | 4.59 | 277.42 |
| Nod-Max. | 89.59 | 91.24 | 32.51 | 105.26 | 172.52 | 176.63 | 84.55 | 15.51 | 621.83 |
| Nod-Mean | 73.27 | 62.03 | 26.34 | 89.77 | 138.59 | 98.11 | 59.67 | 12.66 | 451.18 |
| Nod-RSD | 0.1 | 0.17 | 0.15 | 0.09 | 0.11 | 0.28 | 0.21 | 0.22 | 0.21 |
| Soil-Min. | 68.12 | 48.82 | 21.6 | 76.39 | 121.16 | 69.69 | 40.76 | 1.54 | 319.51 |
| Soil-Max. | 90.58 | 65.42 | 30.09 | 112.78 | 371.71 | 156.57 | 110.47 | 16.3 | 568.73 |
| Soil-Mean | 78.67 | 58.58 | 25.16 | 91.65 | 291.94 | 121.1 | 70.49 | 12.55 | 416.25 |
| Soil-RSD | 0.08 | 0.09 | 0.11 | 0.12 | 0.24 | 0.22 | 0.72 | 0.26 | 0.14 |
| Cer-Min. | 65.32 | 50.17 | 22.79 | 72.97 | 165.67 | 31.62 | 37.02 | 6.28 | 283.67 |
| Cer-Max. | 187.55 | 96.06 | 36.04 | 110.61 | 323.07 | 171.51 | 470.56 | 18.92 | 591.16 |
| Cer-Mean | 94.57 | 69.28 | 26.58 | 84.47 | 243.84 | 92.01 | 102 | 12.9 | 413.21 |
| Cer-RSD | 0.36 | 0.16 | 0.14 | 0.12 | 0.23 | 0.49 | 1.21 | 0.33 | 0.23 |
| Conover-Iman's test <i>p</i> value | | | | | | | | | |
| Soil—Cer | 0.516 | 0.003 | 0.465 | 0.059 | 0.073 | 0.047 | 0.468 | 0.73 | 0.967 |
| Nod—Soil | 0.046 | 0.463 | 0.188 | 0.811 | <0.0001 | 0.062 | 0.066 | 0.94 | 0.411 |
| Nod—Cer | 0.017 | 0.017 | 0.648 | 0.092 | <0.0001 | 0.739 | 0.342 | 0.68 | 0.437 |

Note: The pairwise statistical group differences detected by Conover-Iman's test are given as *p*-values passing the significance threshold of 0.05 highlighted in gray.

Abbreviation: RSD, relative standard deviation.

The similar concentrations of Mn and Fe in the soil samples and the nodules seem to negate the hypothesis of Mn–Fe accumulation as the origin of the nodules.

A Principal Component Analysis (PCA) was performed using Additive Log Ratio (ALR) transformed data with varimax rotation (Figure 6a). Silicon was used as a common divisor because this element had the lowest coefficient of variation. The varimax rotation led to the creation of a *varifactor* that maximizes the sum of the variance of the squared loadings. The aim was to establish stronger associations between the factors and the most meaningful variables for a better interpretation of the results (Pasquet et al., 2016; Reimann et al., 2002). Assuming that the high variation of Zn was mainly arising from the differences in the organic matter content of the samples, this element is added as a supplementary variable that is not loaded on the biplot.

The first two principal components explain 74.5% of the variability in the data set. The similar compositions of the sediment samples and the nodules cause an agglomeration in the center of the biplot with an overlap of the two confidence ellipses. Almost all the ceramic samples do not fit in the two ellipses and are distinct from the sediment samples and the nodules. Only one ceramic sample (coarse ware ceramic) is located inside the ellipses of the nodules and sediment samples.

The difference between the sediment samples and nodules on one side and the ceramics on the other, is mostly noticeable on

the Principal Component 2, which is mainly determined by the contributions of the elements Al (16.6%), Ti (17.3%), Mg (10.2%), V (10.5%), and Cr (13.2%). The distances between the samples within the three data sets are mostly arising from Principal Component 1, which is determined by major contributions from the elements K (16.7%), Fe (9.8%), Rb (13.0%), Sr (10.3%), and Ba (10.8%). On this axis, the distances between the samples in the sediment and nodules groups are short. The distances between the ceramic samples are more pronounced, reflecting their compositional heterogeneity.

Even though PCA was used successfully to describe the geochemical variations between the samples, and to differentiate between the nodules, the surrounding sediment samples, and the ceramics, a significant proportion of the variation of the data set is not mapped. Hierarchical Ascendant Clustering (HAC) analysis was performed on the first five principal components of the PCA, which represent almost 90% of the total variance of the data set. The dendrogram (Figure 6b) shows a clear partitioning in three clusters. Clusters 1 and 2 group only the nodules and the surrounding sediment samples, except for one ceramic sample. Cluster 3 groups all the ceramic samples, as well as two surrounding sediment samples. This result confirms the observations made on PCA about the possibility to discriminate between these three types of samples based on elemental analysis. The presence of two surrounding sediment samples in Cluster 3 is attributed to the high variability of the ceramic elemental composition.

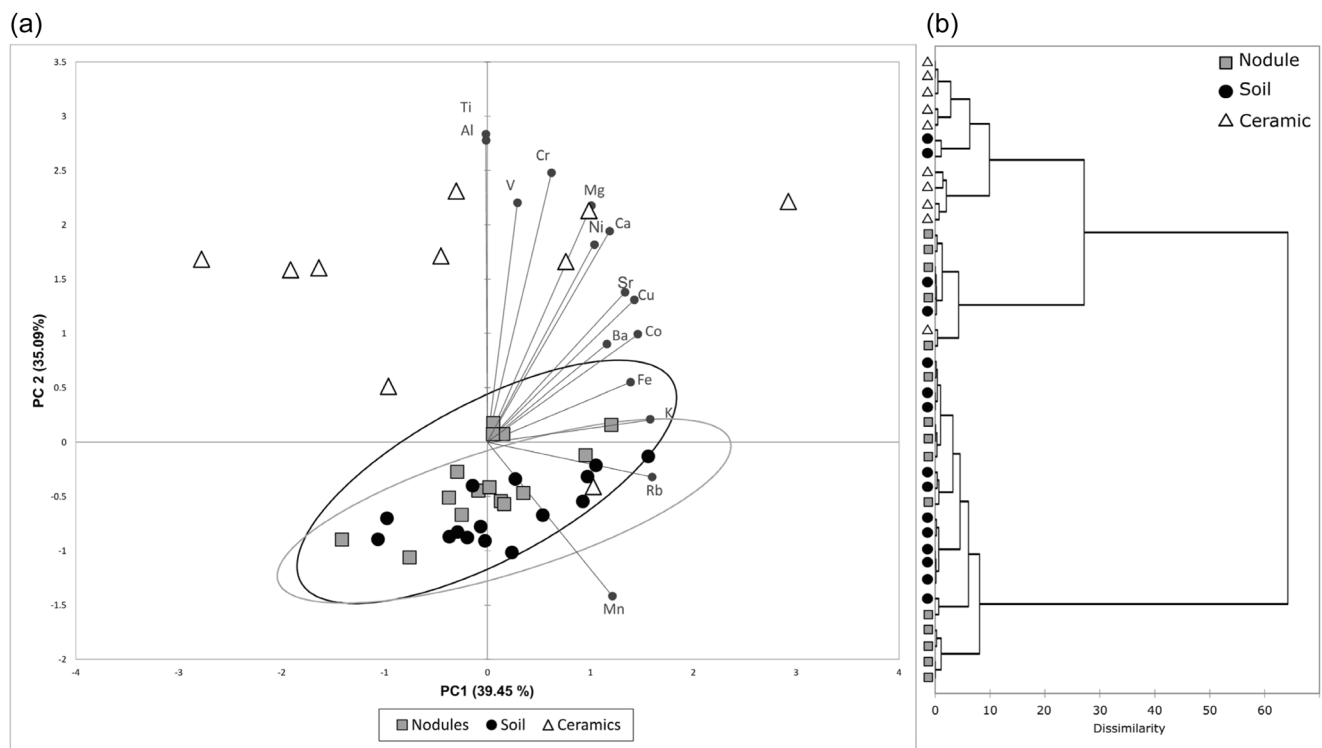


FIGURE 6 (a) PCA plot after ALR transformation and varimax rotation. The plot shows the repartition of the three types of samples in PC1 (D1) and PC2 (D2). The gray and black ellipses show 95% Fisher confidence ellipses of nodules and soil samples, respectively. (b) Dendrogram from hierarchical clustering analysis using Euclidian distance and Ward's aggregation method. ALR, additive log ratio; PCA, principal component analysis.

5.3 | XRD results

The diffractograms in Figure 7 show relevant examples of the sample mineralogy. Typically, the mineral compositions of the nodules and the surrounding sediments are quite similar, with a mineralogical cortege dominated by quartz and feldspars. The other peaks demonstrate the presence of phyllosilicates and iron oxides (hematite or proto-hematite). However, several samples show differences between the nodules and the surrounding sediment in relation to the thermal behavior of the minerals present in these samples.

A pattern reflecting high firing temperatures is shown by samples 244 and E14. Here, the mineral phases identified in the nodule diffractograms are different from the ones detected in the sediment and the experimental nodules. The $d_{(001)}$ peak of kaolinite at $12.4^\circ 2\theta$ was detected in the two sediment samples only. The absence of a kaolinite peak in the experimental nodule is in agreement with the $500\text{--}600^\circ\text{C}$ -dehydroxylation temperature range (Cultrone et al., 2001; McConville & Lee, 2005). The phyllosilicate peak located at $19.8^\circ 2\theta$ was present in both the surrounding sediments and the experimental nodules, with very little difference in their intensity, while it was absent in the nodule diffractograms. Dehydroxylation of phyllosilicates strongly depends on the crystal size and chemical composition. While the illite structure breaks down between 700°C and 800°C , coarse grains of muscovite can withstand temperatures above 900°C (Jordán et al., 1999; McConville & Lee, 2005). The $d_{(104)}$ and $d_{(110)}$ peaks of hematite, located at 33.2° and $35.6^\circ 2\theta$, respectively, were only present in the nodule sample. A wide range

of temperatures can be found in the literature for the growth and formation of hematite, but the lower limit in noncalcareous clay is between 700°C and 750°C (Maniatis et al., 1981; Manoharan et al., 2011). The differences observed in the area between 27° and $28^\circ 2\theta$ were related to the dehydroxylation of the illite-like phyllosilicates and probably the thermal transformation of mixed alkali-feldspar and plagioclase. In E14, the high-intensity peak located at $27.5^\circ 2\theta$ might be related to the neoformation of sanidine, a process that usually starts to occur near 700°C . The mineralogical composition of the nodules and the comparison with the surrounding sediments and the experimental nodules suggest a firing temperature above 700° for these two samples. A second pattern reflecting a low firing temperature is shown by samples CV68 and H70.

Here, the mineralogical compositions of the nodules and the sediments are similar. The phyllosilicate peak at $19.8^\circ 2\theta$ was present in all the diffractograms, and hematite was not detected in any of the diffractograms. In H70, the $d_{(001)}$ peak of kaolinite at $12.4^\circ 2\theta$ was detected in the nodule and in the sediment diffractograms, while it was absent in the experimentally fired soil. This sample also showed a high-intensity $d_{(104)}$ calcite peak at $29.4^\circ 2\theta$ in the nodule diffractogram and a $d_{(104)}$ dolomite peak in the sediment diffractogram. The high-intensity peak located at $27.4^\circ 2\theta$ in the sediment diffractogram was likely related to the presence of alkali-feldspar. The detection of kaolinite in CV68 suggests a firing temperature below 500°C . In H70, the persistence of the calcite peak and the dihydroxylation of kaolinite suggest a firing temperature slightly higher than 500°C .

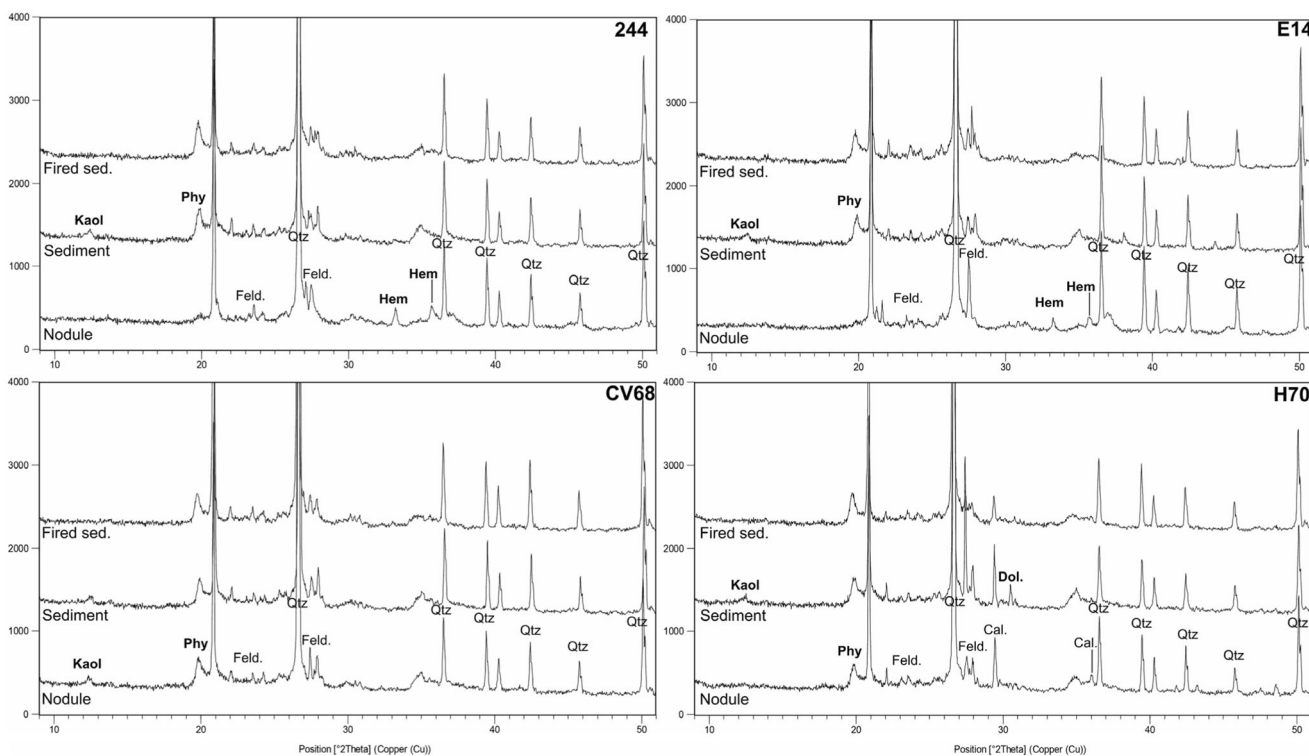


FIGURE 7 Diffractograms of four pairs of nodules, surrounding soil samples, and soil fired at 500°C . Feld, feldspars; Hem, hematite; Kaol, kaolinite; Phy, phyllosilicates; Qtz, quartz.

5.4 | Dating

The TL and radiocarbon results are listed in Table 2. The comparison between TL dates and radiocarbon dates is shown in Figure 8.

Six of the nodules have dates between 1000 and 1200 CE. Nodules NOD-CV68 and NOD-CV48 are older than these and are dated to 954 ± 100 CE and AD 764 ± 134 CE, respectively. However, sample CV68 could also be from the 1000s according to the 100-year uncertainty calculated. Samples NOD-E14 and NOD-G20 are

younger, dated to 1330 ± 62 CE and 1820 ± 34 CE, respectively. Nodule NOD-G20 is the only one obtained from a pit located in a charcoal kiln platform. This red nodule was found among a large majority of small blackened nodules, and the date indicates formation simultaneously with modern charcoal production.

The results of the radiocarbon dating show that sample CHAR-G22 (906–1023 CE, 1σ) matched the date ranges of four TL dates. However, the date of sample CHAR-244 (1521–1641 CE, 1σ) did not match the dates of the nodules, and the date of sample CHAR-E27

TABLE 2 Dates of the 10 nodules measured with thermoluminescence

| Sample name | Dose (Gy) | Dose rate (μGy/year) | Date (AD) | 1σ | U-Nod (μg g ⁻¹) | Th-Nod (μg g ⁻¹) | K-Nod (wt%) | U-Sed (μg g ⁻¹) | Th-Sed (μg g ⁻¹) | K-Sed (wt%) |
|--------------------|-------------|----------------------|-----------|-----|-----------------------------|------------------------------|-------------|-----------------------------|------------------------------|-------------|
| TL-dating | | | | | | | | | | |
| NOD-H41 | 3.63 (0.02) | 3523 (436) | 1072 | 103 | 2.2 | 18.1 | 1.44 | 1.3 | 9.9 | 1.36 |
| NOD-G22 | 3.31 (0.06) | 3433 (320) | 1126 | 88 | 2.13 | 12.49 | 1.42 | 2.1 | 11.8 | 1.49 |
| NOD-E14 | 2.83 (0.04) | 3641 (394) | 1330 | 62 | 2.17 | 13.04 | 1.17 | 2.33 | 14.4 | 1.29 |
| NOD-G20 | 1.68 (0.08) | 3346 (402) | 1820 | 34 | 1.96 | 15.55 | 1.55 | 2 | 12.1 | 1.69 |
| NOD-H70 | 3.81 (0.03) | 3714 (413) | 1153 | 71 | 1.85 | 12.65 | 1.81 | 2.04 | 11.7 | 1.85 |
| NOD-244 | 3.90 (0.03) | 3435 (410) | 1055 | 103 | 2.2 | 13.8 | 1.48 | 1.71 | 11 | 1.48 |
| NOD-XP1H3 | 3.82 (0.16) | 3514 (394) | 1096 | 88 | 2.12 | 12.33 | 1.62 | 1.6 | 9.13 | 1.84 |
| NOD-ZP5H2 | 3.69 (0.04) | 3407 (412) | 1121 | 79 | 1.91 | 13.36 | 1.49 | 2.04 | 12.4 | 1.49 |
| NOD-CV68 | 4.08 (0.05) | 3562 (387) | 964 | 100 | 1.79 | 12.36 | 1.41 | 2.33 | 13.3 | 1.41 |
| NOD-CV48 | 4.86 (0.09) | 3891 (417) | 765 | 138 | 2.05 | 13.66 | 1.48 | 2.41 | 13.5 | 1.69 |
| Radiocarbon dating | | | | | | | | | | |
| Sample name | 14C-age | | | | Calib. date CE, 1σ | | | | | |
| CHAR-E27 | 215 ± 27 | | | | 1650–1949 | | | | | |
| CHAR-244 | 309 ± 28 | | | | 1521–1641 | | | | | |
| CHAR-G22 | 1059 ± 30 | | | | 906–1023 | | | | | |

Note: Dose, dose rate, and the concentration of radioactive elements used for the calculation of the age are also listed.

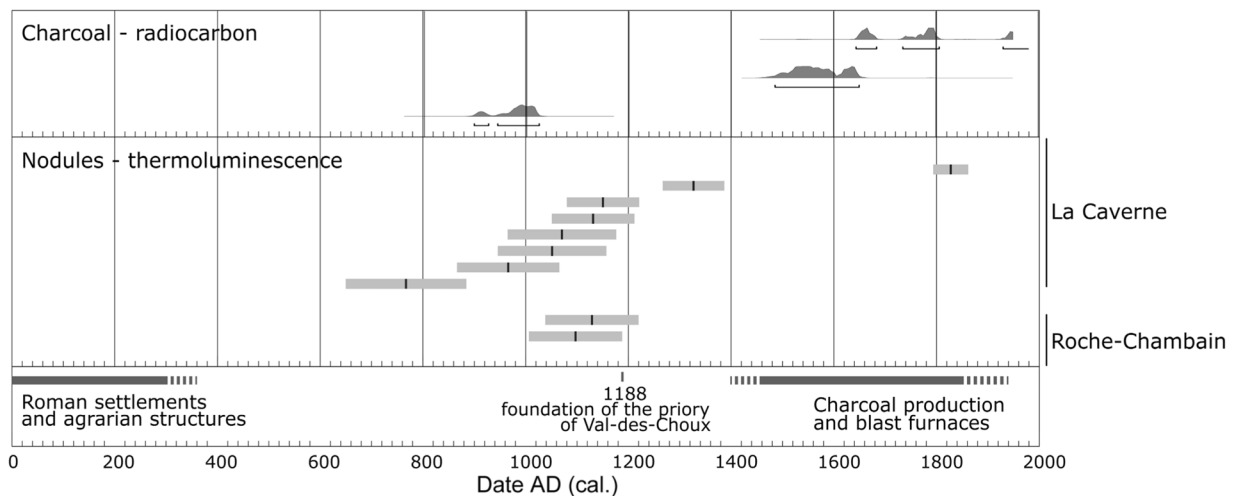


FIGURE 8 TL dates of the 10 nodules and radiocarbon dates of the 3 charcoal fragments.

(1650–1949 CE, 1 σ) was close to the modern TL date of nodule NOD-G20, collected near a charcoal burning area.

6 | DISCUSSION

6.1 | Origin of the nodules

The similarities observed between the chemical and mineralogical compositions of the nodules and the soil indicate that the nodules represent an aggregation of the local sediment. Indeed, the wide dispersion of the ceramic samples in the PCA plot and their aggregation in the HAC dendrogram reflect varied elemental compositions, in general, quite different from the nodules and the sediment compositions. Furthermore, this indicates that the raw materials used to make the ceramics were very different from the local soil. Considering the quite broad chronology of the ceramics and their compositional diversity, the sherds likely originated from different production centers. It should be noted that this area of Burgundy is well known for not using roof tiles in the Roman period. Instead, the roof tiles were usually made of local stones, mainly limestone (Delencre & Garcia, 2014). The chemical analyses do not support the hypothesis that the nodules could be the results of Mn or Fe concretions in the soil, as the concentrations of these two elements are not higher in the nodules than in the surrounding soil. Because of the formation process, such types of concretions are usually enriched 30–60 times in Mn with respect to the surrounding soil, and more moderately in Fe (Gasparatos, 2011). Moreover, the samples observed in thin sections do not show the characteristic concentric internal structures that can be present in Mn and Fe concretions.

The hypothesis of the indurated nodule being weathered remains of burnt earth building materials such as adobe or rammed earth has been considered, but several reasons led us to rule out this idea. The first argument is a chronological one. Indeed, the finding of burnt earth building materials could be likely related to the occupation period of the sites, between 5th century BC and 5th century CE. However, the dating of the indurated nodules, mostly between 1000 and 1200 CE, does not match with the dates of the structures and artifacts discovered. On the two sites of this study, the latest identified coin was located in the Roman building on the Roche-Chambain site and was dated back to 193 CE. On the LiDAR map, most of the features are observed in connection with the Roman settlements and a few features are not dated. Ultimately, it could be argued that later buildings made of perishable materials might have been constructed in this area, but no evidence or hint of medieval occupation has been found at the time of this study. These data suggest that these lands were used by the people of the medieval period living in the village surrounding the forest or in the Commandery.

Regarding the distributions of these nodules, it must be emphasized that they were found in nearly 60% of the pits opened on an area of about 1.62 km², with no preferential distribution. Moreover, their distribution is totally independent of the structure

locations and the archaeological artifacts collected during surveys. If the nodules were indeed remains of burnt earth building materials, high-density spots close to artifacts or anthropic structures would be expected. Mechanical processes like plowing could have perturbed the distribution and the morphology of the remains on the cultivated parcels (Sherwood et al., 1995), but the delineations between the parcels would have prevented large-scale scattering. If bioturbation could be considered to be responsible for the fragmentation of burnt earth building materials and their vertical scattering in soils, the spatial distribution would only be minimally impacted.

From a chemical perspective, the PCA plot (Figure 6) shows that the confidence ellipses of the nodules and the surrounding sediments are almost overlapping, reflecting very similar variability. If the nodules were fragments of earth building materials, a higher chemical homogeneity linked to the use of a common clay material source would be expected.

Even though the analytic results showed that the nodules likely originated from the aggregation of local sediment, the analysis of the elemental composition showed significant differences in Zn, Al, and Ti concentrations. The Zn concentration of soils usually depends on the parent material mineralogy, pH, texture, and content of organic matter (Salminen et al., 2005). In the present context, the difference in Zn concentrations between 104 $\mu\text{g g}^{-1}$ (minimum in nodules) and 371 $\mu\text{g g}^{-1}$ (maximum in soil samples) was assumed to be the result of differences in the content of organic matter. Indeed, the forest soil was enriched in organic matter through plant exudates, dissolved organic matter, and bioturbation processes (Egli et al., 1999; Rumpel & Kögel-Knabner, 2010). Moreover, the lower external porosity of the indurated nodules would not allow the infiltration of organic matter into their structure. No satisfactory explanation has been found to explain the differences in Al and Ti concentrations.

6.2 | Relationship with agricultural practices

The nodules were mainly found within the limits of Roman parcels, but their locations were scattered in the study area and some of them were also found outside of the parcels. Most of them were not found in relation with other archaeological structures or archaeological artifacts; thus, they are unlikely to be related to artisanal or funerary fire activities. Yet, they could be linked to fires instigated by humans as part of agricultural practices or to natural wildfire. In the latter case, some studies refer to the formation of reddened baked clay fragments or superficial rubification of soils, linked to a high amount of fuel (Goforth et al., 2005; Parson et al., 2010). However, because soils are generally poor conductors of heat, these features are typically limited to the first few centimeters of organo-mineral horizons (Mataix-Solera et al., 2011). Furthermore, the effects seem to be relatively minimal at the scale of a single wildfire and more likely associated with high-severity ones. Because some of the reddish-baked nodules discovered in the forest of Châtillon were rather large, and in all likelihood heated above 500°C, they probably correspond

to a fire of particular intensity. The limited spatial recurrence and the relatively broad dating range over c. 500 years suggest that several firing events were repeated at the same location, which seems less congruent with the natural fire hypothesis in this temperate continental context.

Therefore, the case of agricultural fires should be considered. While surface fires such as the ones resulting from natural wildfires and the slash-and-burn practice tend not to lead to severe burning of the ground surface (Ehrmann et al., 2014; Ponomarenko et al., 2019; Schulz et al., 2014), more complex agricultural fire techniques such as paring and burning can result in a high temperature that would affect soil structure and mineralogy to a higher degree (Menbrivès et al., 2019). Because it involves soil surface extraction and firing within kiln-like structures, this operation intentionally produces significant baking of the mineral soil fraction (Guiblais-Starck et al., 2020; Jobbé-Duval, et al., 2007; Nicolai, 1961; Nzila, 1992). This type of fire practice was used in temporary cropping systems or permanent ones that include pasture. This first step was usually undertaken to clear the soil surface before cultivation and can be repeated in rotational cycles of several decades (Sigaut, 1975). The model proposed here appears to be more consistent with our results and explains their chronology and spatial recurrence in a more satisfactory manner.

6.3 | A vestige of the medieval agricultural evolution

The chronological discrepancy between the dates of the nodules and the archaeological structures from the Gallo-Roman period was probably the most surprising feature of this study. Indeed, the proximity of a Roman villa dated from the 1st and 2nd centuries AD (Provost, 2009a, 2009b) complicated the chronology of the fire events. Except for sample E-14, all the nodules span a chronological range from the 8th to the 14th century and they are roughly concentrated between AD 1000 and 1200. This period corresponds to a time when land occupation and the organization of farming drastically changed in Western Europe. During this period of agricultural evolution, technological innovations such as the gradual adoption of the 3-year crop rotation system, the increasing use of iron for agrarian tools, and the widespread development of moldboard plows made it possible to establish a new socioeconomic system leading to increased productivity (Duby, 1954; Grenand, 1996). This evolution was also characterized by an expansion of the area of land dedicated to cultivation. With the technological progress and higher production rates, people started to turn to the unexploited forest soils. This period was indeed seen as a time when the forest receded to make way for more cultivated land (Mazoyer & Roudart, 2017). The development of the monastic network was also seen as an important factor in the land clearing process (Bloch, 1931; Bechmann, 1981, 1984). Because the medieval nodules were mostly found inside the limits of Gallo-Roman parcels, these results suggest that in this case, medieval peasants used the structures already implemented rather than delimiting new field spaces. Thus, the uses

of this newly cleared land still need to be determined. The finding of small metal bells for cattle seems to point to the practice of pastoralism (Giosa, 2020), but further investigations of the housing structures are needed to confirm this.

The hypothesis of agricultural fires is congruent with the detection of post-Gallo-Roman agrarian parcels on the plateau, while medieval occupations are mostly documented in valleys surrounding the forest. Even though the development of the monastic networks is often seen as an important factor in the medieval land clearing process, in the Châtillon forest, the nodules indicate the use of agricultural fire practice prior to the monastic implantation. The chronology appears not to be congruent with a unique phase of woodland clearance, but better supports the possibility of multiple clearing fires as part of a shifting or temporary agricultural management, such as paring-and-burning. Moreover, our dates support the possibility that the foundation of the monasteries resulted in a modification in forest use rights, and a diminution of temporary agricultural clearings.

7 | CONCLUSION

This study provides the identification of a new ecofact related to agricultural fire practices in medieval times. Although the practice of land clearance in association with fire has previously generally only been characterized from indirect proxies such as palynological cores. The elemental and mineralogical analyses undertaken in this study showed that the indurated nodules were formed from the rubefaction of the local sediment. Even though the origin of the fire cannot be precisely determined from the composition of the nodules, several observations suggest the use of the “paring-and-burning” technique. Indeed, the high firing temperatures shown by their mineralogy do not correspond with that of temperate natural wildfires. The fragmented shapes, rather than a homogeneous reddened surface layer, indicate that the soil was mechanically worked before and/or after the fire event. Moreover, the chronological range of the nodules provided by the TL-dating matches the evolution of agricultural practices during medieval times. Currently ongoing environmental studies focused on soil chemistry, seed, and pollen from this area will help to specify which agricultural activities were practiced. The identification of anthropic fire used for agricultural purposes is an important question for archaeologists and paleoecologists. It can shed new light on the evolution of the landscapes and provide useful information on the relationships between humans and their environment in relation to agricultural systems. Even if these types of artifacts can be difficult to detect, we hope that this study will raise awareness on the necessity to track and analyze such combustion traits.

ACKNOWLEDGEMENTS

This study has been partially funded by a PhD grant awarded to Alain Giosa by the University Paris 1 Panthéon-Sorbonne. The authors would like to thank the anonymous reviewers and the review editor, whose comments helped us to significantly improve this article.

ORCID

Thomas Delbey  <https://orcid.org/0000-0001-7308-0580>

Clément Menbrivès  <https://orcid.org/0000-0002-9874-1274>

Kaare L. Rasmussen  <http://orcid.org/0000-0001-9575-868X>

REFERENCES

- Aldeias, V. (2017). Experimental approaches to archaeological fire features and their behavioral relevance. *Current Anthropology*, 58(16), 191–205. <https://doi.org/10.1086/691210>
- Baize, D. (2012). Les "terres d'Aubues" de Basse Bourgogne. *Étude et Gestion des Sols*, 19(3), 139–161.
- Baize, D., & Jabiol, B. (1995). *Guide pour la description des sols*. Editions Quae.
- Bechmann, R. (1981). *Les racines des cathédrales: l'architecture gothique, expression des conditions du milieu*. Bibliothèque Historique Payot.
- Bechmann, R. (1984). *Des arbres et des hommes: la forêt au Moyen-Âge*. Flammarion.
- Beck, C., & Beck, P. (2007). L'exploitation et la gestion des ressources naturelles dans le domaine ducal Bourguignon à la fin du XIVe siècle. *Médiévales*, 53, 93–108. <https://doi.org/10.4000/medievales.3863>
- Benoît, S., & Rignault, B. (1988). Le patrimoine sidérurgique du Châtillonnais Châtillonnais. *Mémoires de la Commission des antiquités du département de la Côte-d'Or*, n° 34, 1984–1986, pp. 387–448.
- Bentsen, S. E. (2013). Using pyrotechnology: Fire-related features and activities with a focus on the african middle stone age. *Journal of Archaeological Research*, 22(2), 141–175. <https://doi.org/10.1007/s10814-013-9069-x>
- Bloch, M. (1931). Les caractères originaux de l'histoire rurale française. *Bulletin de l'Association Guillaume Budé*, 33, 56–62.
- Brain, C. K., & Sillent, A. (1988). Evidence from the Swartkrans Cave for the earliest use of fire. *Nature*, 336(6198), 464–466. <https://doi.org/10.1038/336464a0>
- Canti, M., & Linford, N. (2000). The effects of fire on archaeological soils and sediments: Temperature and colour relationships. *Proceedings of the Prehistoric Society*, 66, 385–395. <https://doi.org/10.1017/s0079497x00001869>
- Certini, G. (2005). Effects of fire on properties of forest soils: A review. *Oecologia*, 143(1), 1–10. <https://doi.org/10.1007/s00442-004-1788-8>
- Chaume, B. (1999). Les ensembles funéraires de Lt A dans le Châtillonnais: Eléments d'une problématique pour un autre regard sur la transition Hallstatt-La Tène. *Germania: Anzeiger der Römisch-Germanischen Kommission des Deutschen Archäologischen Instituts*, 77(2), 489–566.
- Chevigny, E., Saligny, L., Granjon, L., Goguy, D., Cordier, A., Pautrat, Y., & Giosa, A. (2018). Identifier et enregistrer des vestiges archéologiques sous couvert Forestier à partir de données LiDAR: méthode et limites. *ArchéoSciences*, 42(2018), 31–43. <https://doi.org/10.4000/archeosciences.5727>
- Chevrier, S. (2011). *Meulson, Côte d'Or, Le Grand Chemin Un enclos funéraire du Second âge du Fer de la haute vallée de la Seine : diagnostic archéologique*, Rapport final d'opération, Dijon, INRAP Grand Est Sud, 86 p.
- Cruz, F. (2012). *L'environnement du site « princier » de Vix (Côte d'Or): Approche géoarchéologique* [Doctoral dissertation, Université de Bourgogne].
- Cultrone, G., Rodriguez-Navarro, C., Sebastian, E., Cazalla, O., & De La Torre, M. J. (2001). Carbonate and silicate phase reactions during ceramic firing. *European Journal of Mineralogy*, 13(3), 621–634. <https://doi.org/10.1127/0935-1221/2001/0013-0621>
- Delencre, F., & Garcia, J. P. (2014). Apparition et adoption des matériaux de couverture romains chez les Eduens et chez les Lingons. *Archäologisches Korrespondenzblatt*, 44, 395–411.
- Duby, G. (1954). La révolution agricole médiévale. *Revue de géographie de Lyon*, 29(4), 361–366. <https://doi.org/10.3406/geoca.1954.2010>
- Durcan, J. A., King, G. E., & Duller, G. A. T. (2015). DRAC: Dose Rate and Age Calculator for trapped charge dating. *Quaternary Geochronology*, 28, 54–61. <https://doi.org/10.1016/j.quageo.2015.03.012>
- Egli, M., Fitze, P., & Oswald, M. (1999). Changes in heavy metal contents in an acidic forest soil affected by depletion of soil organic matter within the time span 1969–93. *Environmental Pollution*, 105(3), 367–379. [https://doi.org/10.1016/s0269-7491\(99\)00040-8](https://doi.org/10.1016/s0269-7491(99)00040-8)
- Ehrmann, O., Biester, H., Bogenrieder, A., & Rösch, M. (2014). Fifteen years of the Forchtenberg experiment—results and implications for the understanding of Neolithic land use. *Vegetation History and Archaeobotany*, 23(S1), 5–18. <https://doi.org/10.1007/s00334014-0452-4>
- Fitzpatrick, R. W. (1988). Iron compounds as indicators of Pedogenic processes: Examples from the Southern hemisphere. In J. W. Stucki, B. A. Goodman, & U. Schwertmann (Eds.), *Iron in soils and clay minerals* (pp. 351–396). Springer. https://doi.org/10.1007/978-94-009-4007-9_13
- Gasparatos, D. (2011). Fe–Mn concretions and nodules to sequester heavy metals in soils. In E. Lichtfouse, J. Schwarzbauer, & D. Robert (Eds.), *Environmental chemistry for a sustainable world* (pp. 443–474). Springer. https://doi.org/10.1007/978-94-007-2439-6_11
- Georges-Leroy, M. (2009). L'apport du laser scanner aéroporté à l'étude des parcelles gallo-romaines du massif forestier de Haye (Meurthe-et-Moselle). *Archéométrie 2009—Ressources, Sociétés, Biodiversité. Colloque du GMPCA*.
- Georges-Leroy, M., Bock, J., Dambrine, É., & Dupouey, J. (2011). Apport du LiDAR à la connaissance de l'histoire de l'occupation du Sol en Forêt de Haye. *ArchéoSciences*, 35, 117–119. <https://doi.org/10.4000/archeosciences.3015>
- Giosa, A. (2020). *Les agrosystèmes antiques du Châtillonnais: Approche archéopédologique de la mémoire des forêts dans les parcelles reconnues par télédétection LiDAR* [Doctoral dissertation, University Paris 1 Panthéon-Sorbonne].
- Goforth, B. R., Graham, R. C., Hubbert, K. R., Zanner, C. W., & Minnick, R. A. (2005). Spatial distribution and properties of ash and thermally altered soils after high-severity forest fire, Southern California. *International Journal of Wildland Fire*, 14(4), 343. <https://doi.org/10.1071/wf05038>
- Goguy, D., Bénard, J., Berranger, M., Chevigny, E., Fovet, E., Giosa, A., & Petit, C. (2018). *Structures en pierre du plateau du Châtillonnais (Côte-d'Or): Du Hallstatt à l'Antiquité tardive: l'apport de l'archéologie forestière*. Éditions Mergoil.
- Goguy, D., Cordier, A., & Chevigny, E. (2014, May). Typologie des enclos dans les forêts du Châtillonnais (Côte d'Or). *Séminaire Workshop 2 Les parcelles conservés sous forêt*, Available from HAL archives-ouvertes.fr: halshs-01053247v2f
- Goguy, D., Pautrat, Y., Guillaumet, J. P., Thevenot, J. P., & Popovitch, L. (2010). Dix ans d'archéologie forestière dans le Châtillonnais (Côte-d'Or): Enclos, habitats, parcelles. *Revue Archéologique de l'Est*, 59–1, 99–211.
- Golitzko, M., & Terrell, J. E. (2012). Mapping prehistoric social fields on the Sepik coast of Papua New Guinea: Ceramic compositional analysis using laser ablation-inductively coupled plasma-mass spectrometry. *Journal of Archaeological Science*, 39(12), 3568–3580. <https://doi.org/10.1016/j.jas.2012.05.037>
- Grenand, F. (1996). L'abattis contre l'essart, again. *Journal D'agriculture Traditionnelle et de Botanique Appliquée*, 38(1), 19–53. <https://doi.org/10.3406/jatba.1996.3586>
- Grün, R. (2009). The DATA program for the calculation of ESR age estimates on tooth enamel. *Quaternary Geochronology*, 4(3), 231–232. <https://doi.org/10.1016/j.quageo.2008.12.005>
- Gualtieri, A. F., & Venturelli, P. (1999). In situ study of the goethite-hematite phase transformation by real time synchrotron powder diffraction. *American Mineralogist*, 84(5–6), 895–904. <https://doi.org/10.2138/am-1999-5-624>

- Guiblais-Starck, A., Menbrivès, C., Coubray, S., Dandurand, G., Giosa, A., Martin, S., & Petit, C. (2020). Première identification archéologique d'un écobuage médiéval: Le site de Vaudes—Les Trappes—(Aube). *ArchéoSciences*, (44), 219–235. <https://doi.org/10.4000/archeosciences.7900>
- Hong, D., Kim, M., Choi, J., El-Faramawy, N., & Göksu, H. (2006). Equivalent dose determination of single aliquot regenerative-dose (SAR) protocol using thermoluminescence on heated quartz. *Nuclear Instruments and Methods in Physics Research Section B: Beam Interactions with Materials and Atoms*, 243(1), 174–178. <https://doi.org/10.1016/j.nimb.2005.05.059>
- Jean de Dieu, N. (1992). *La pratique de l'écobuage dans la vallée du Niari (Congo): Ses conséquences sur l'évolution d'un sol ferrallitique acide*. ORSTOM.
- Jobbé-Duval, M., Cochet, H., & Bourliaud, J. B. (2007). L'écobuage andin. Questions sur les origines, l'extension, les modalités et le devenir d'une technique d'ouverture des champs de pomme de terre sur puna humide (Cochabamba, Bolivie). *Techniques & Culture. Revue semestrielle d'anthropologie des techniques*, 149–188
- Johnson, D. W., & Curtis, P. S. (2001). Effects of forest management on soil C and N storage: Meta analysis. *Forest Ecology and Management*, 140(2–3), 227–238. [https://doi.org/10.1016/s0378-1127\(00\)00282-6](https://doi.org/10.1016/s0378-1127(00)00282-6)
- Jordán, M., Boix, A., Sanfeliu, T., & De la Fuente, C. (1999). Firing transformations of Cretaceous clays used in the manufacturing of ceramic tiles. *Applied Clay Science*, 14(4), 225–234. [https://doi.org/10.1016/s0169-1317\(98\)00052-0](https://doi.org/10.1016/s0169-1317(98)00052-0)
- Ketterings, Q. M., Bigham, J. M., & Laperche, V. (2000). Changes in soil mineralogy and texture caused by slash-and-burn fires in Sumatra, Indonesia. *Soil Science Society of America Journal*, 64(3), 1108–1117. <https://doi.org/10.2136/sssaj2000.6431108x>
- Kreutzer, S., Schmidt, C., Fuchs, M. C., Dietze, M., Fischer, M., & Fuchs, M. (2012). Introducing an R package for luminescence dating analysis. *Ancient TL*, 30(1), 1–8.
- Latrille, C., Elsass, F., Van Oort, F., & Denaix, L. (2001). Physical speciation of trace metals in Fe–Mn concretions from a rendzic lithosol developed on Sinemurian limestones (France). *Geoderma*, 100(1–2), 127–146. [https://doi.org/10.1016/s0016-7061\(00\)00083-5](https://doi.org/10.1016/s0016-7061(00)00083-5)
- Leneuf, N., & Puisségur, J. J. (1976). Minéraux argileux et conditions paléocéologiques dans les dépôts quaternaires de versants, en Bourgogne. *Bulletin de l'Association Française Pour l'étude du Quaternaire*, 13(3), 145–156. <https://doi.org/10.3406/quate.1976.1289>
- Liritzis, I., Kitis, G., Galloway, R. B., Vafiadou, A., Tsirliganis, N., & Polymeris, G. (2008). Probing luminescence dating of archaeologically significant carved rock types. *Mediterranean Archaeology and Archaeometry*, 8(1), 61–79.
- Macphail, R., & Goldberg, P. (1990). The micromorphology of tree subsoil hollows: Their significance to soil science and archaeology. *Developments in Soil Science*, 19, 425–429. [https://doi.org/10.1016/s0166-2481\(08\)70357-x](https://doi.org/10.1016/s0166-2481(08)70357-x)
- Macphail, R. I., Courty, M. A., & Gebhardt, A. (1990). Soil micromorphological evidence of early agriculture in north-west Europe. *World Archaeology*, 22(1), 53–69. <https://doi.org/10.1080/00438243.1990.9980129>
- Maniatis, Y., Simopoulos, A., & Kostikas, A. (1981). Moessbauer study of the effect of calcium content on iron oxide transformations in fired clays. *Journal of the American Ceramic Society*, 64(5), 263–269. <https://doi.org/10.1111/j.1151-2916.1981.tb09599.x>
- Manoharan, C., Sutharsan, P., Dhanapandian, S., Venkatchalapathy, R., & Asanulla, R. M. (2011). Analysis of temperature effect on ceramic brick production from alluvial deposits, Tamilnadu, India. *Applied Clay Science*, 54(1), 20–25. <https://doi.org/10.1016/j.clay.2011.07.002>
- Mataix-Solera, J., Cerdà, A., Arcenegui, V., Jordán, A., & Zavala, L. (2011). Fire effects on soil aggregation: A review. *Earth-Science Reviews*, 109(1–2), 44–60. <https://doi.org/10.1016/j.earscirev.2011.08.002>
- Mazoyer, M., & Roudart, L. (2017). *Histoire des agricultures du monde. Du néolithique à la crise contemporaine*. Média Diffusion.
- McConville, C. J., & Lee, W. E. (2005). Microstructural development on firing illite and smectite clays compared with that in kaolinite. *Journal of the American Ceramic Society*, 88(8), 2267–2276. <https://doi.org/10.1111/j.1551-2916.2005.00390.x>
- Menbrivès, C., Christophe, P., Michelle, E., Wassel, E., & Fechner, K. (2019). Feux agricoles, destechiques méconnues des archéologues. L'apport de l'étude archéopédologiques résidus de combustion de Transinne (Belgique). *Soils as records of Past and present: The geoarchaeological approach. Focus on: Is there time for field-work today?* Raakvlak Archaeology, Monuments and Landscapes of Bruges and Hinterland, pp. 121–139.
- Neary, D. G., Klopatek, C. C., DeBano, L. F., & Ffolliott, P. F. (1999). Fire effects on belowground sustainability: A review and synthesis. *Forest Ecology and Management*, 122(1–2), 51–71. [https://doi.org/10.1016/s0378-1127\(99\)00032-8](https://doi.org/10.1016/s0378-1127(99)00032-8)
- Nicloux, C. (1986). *Typologie des stations forestières dans la forêt domaniale de Châtillon-sur-Seine*. E.N.G.R.E.F Nancy.
- Nicolaï, H. (1961). *Luizi: Géographie régionale d'un pays du Bas-Congo*, J. Duculot, Académieroyale des Sciences d'Outre-Mer, Classe des sciences naturelles et médicales, 95.
- Olley, J., Caitcheon, G., & Murray, A. (1998). The distribution of apparent dose as determined by optically stimulated luminescence in small aliquots of fluvial quartz: Implications for dating young sediments. *Quaternary Science Reviews*, 17(11), 1033–1040. [https://doi.org/10.1016/s0277-3791\(97\)00090-5](https://doi.org/10.1016/s0277-3791(97)00090-5)
- Parson, A., Robichaud, P. R., Lewis, S. A., Napper, C., & Clark, J. T. (2010). *Field guide for mapping post-fire soil burn severity*. GTR, U.S. Department of Agriculture, Forest Service, Rocky Mountain Research Station. <https://doi.org/10.2737/rmrs-gtr-243>
- Pasquet, C., Le Monier, P., Monna, F., Durllet, C., Brigaud, B., Losno, R., Chateau, C., Laporte-Magoni, C., & Gunkel-Grillon, P. (2016). *Impact of nickel mining in New Caledonia assessed by compositional data analysis of lichens* (Vol. 5). SpringerPlus. <https://doi.org/10.1186/s40064-016-3681-4>
- Pautrat, Y., & Goguy, D. (2004). État actuel des connaissances sur les sites archéologiques forestiers du Châtillonnais: L'exemple des parcellaires. *La Mémoire des Forêts*, 133, 032115.
- Phillippe, W. R., Blevins, R. L., Barnhisel, R. I., & Bailey, H. H. (1972). Distribution of concretions from selected soils of the inner bluegrass region of Kentucky. *Soil Science Society of America Journal*, 36(1), 171–173. <https://doi.org/10.2136/sssaj1972.03615995003600010055x>
- Poirier, N., & Laüt, L. (2013). Approches comparées du mobilier hors-site: Peut-on cerner l'espace agraire antique?/A comparative approach to offsite artefacts: Is it possible to identify ancient agrarian land? *Supplément à la Revue Archéologique du Centre de la France*, 45(1), 113–133.
- Poirier, N., & Nuninger, L. (2012). Techniques d'amendement agraire et témoins matériels. *Histoire & Sociétés Rurales*, 38(2), 11. <https://doi.org/10.3917/hsr.038.0011>
- Ponomarenko, E., Tomson, P., Ershova, E., & Bakumenko, V. (2019). A multi-proxy analysis of sandy soils in historical slash-and-burn sites: A case study from Southern Estonia. *Quaternary International*, 516, 190–206. <https://doi.org/10.1016/j.quaint.2018.10.016>
- Portères, R. (1972). De l'écobuage comme un système mixte de culture et de production. *Journal d'agriculture tropicale et de botanique appliquée*, 19, 151–207.
- Provost, M. (2009a). *La Côte-d'Or. 3, De Nuits-Saint-Georges à Voullaines-les Templiers*. Académie des inscriptions et belles-lettres: Ministère de l'éducation nationale: Ministère de la Recherche.
- Provost, M. (2009b). *La Côte-d'Or. 2, D'Allerey à Normier*. Académie des inscriptions et belles-lettres: Ministère de l'éducation nationale: Ministère de la Recherche.

- Py, V. (2006). Mine charcoal deposits: Methods and strategies. The medieval Fournel silver mines in the Hautes-Alpes (France). In A. Dufraisse (Ed.), *Charcoal analysis: New analytical tools and methods for archaeology. Papers from the table-ronde held in Basel* (Vol. 1483, pp. 35–46). Archaeopress.
- Rabenhorst, M. C., & Parikh, S. (2000). Propensity of soils to develop redoximorphic color changes. *Soil Science Society of America Journal*, 64(5), 1904–1910. <https://doi.org/10.2136/sssaj2000.6451904x>
- Reimann, C., Filzmoser, P., & Garrett, R. G. (2002). Factor analysis applied to regional geochemical data: Problems and possibilities. *Applied Geochemistry*, 17(3), 185–206. [https://doi.org/10.1016/s0883-2927\(01\)00066-x](https://doi.org/10.1016/s0883-2927(01)00066-x)
- Reimer, P. J., Austin, W. E., Bard, E., Bayliss, A., Blackwell, P. G., Bronk Ramsey, C., Butzin, M., Cheng, H., Edwards, R. L., Friedrich, M., Grootes, P. M., Guilderson, T. P., Hajdas, I., Heaton, T. J., Hogg, A. G., Hughen, K. A., Kromer, B., Manning, S. W., Muscheler, R., & Talamo, S. (2020). The IntCal20 Northern hemisphere radiocarbon age calibration curve (0–55 cal kBP). *Radiocarbon*, 62(4), 725–757. <https://doi.org/10.1017/rdc.2020.41>
- Roduit, N. (2007). *JMicroVision: un logiciel d'analyse d'images pétrographiques polyvalent* [Doctoral dissertation, University of Geneva].
- Roebroeks, W., & Villa, P. (2011). On the earliest evidence for habitual use of fire in Europe. *Proceedings of the National Academy of Sciences*, 108(13), 5209–5214. <https://doi.org/10.1073/pnas.1018116108>
- Röpke, A., & Dietl, C. (2017). Burnt soils and sediments. In C. Nicosia, & G. Stoops (Eds.), *Archaeological soil and sediment micromorphology* (pp. 173–180). Wiley.
- Roserot, A. (1924). Dictionnaire topographique du département de la Côte-d'Or: comprenant les noms de lieux anciens et modernes. Imprimerie Nationale.
- Rumpel, C., & Kögel-Knabner, I. (2010). Deep soil organic matter—A key but poorly understood component of terrestrial C cycle. *Plant and Soil*, 338(1–2), 143–158. <https://doi.org/10.1007/s11104-010-0391-5>
- Salminen, R., (Chief-editor), Batista, M. J., Bidovec, M., Demetriades, A., De Vivo, B., De Vos, W., & Tarvainen, T. (2005). *Geochemical atlas of Europe. Part 1—Background information, methodology and maps*. Geological Survey of Finland.
- Schulz, E., Vannina, U., & Hall, M. (2014). The double mosaic-regeneration of vegetation and soil after clearing, burning, and cultivation: Lessons from the Forchtenberg experiment. *Vegetation History and Archaeobotany*, 23(S1), 19–36. <https://doi.org/10.1007/s00334-014-0451-5>
- Scott, A. C., Bowman, D. M., Bond, W. J., Pyne, S. J., & Alexander, M. E. (2014). *Fire on earth: An introduction*. Wiley-Blackwell.
- Šegvić, B., Girardclos, S., Zanoni, G., Arbiol González, C., Steimer-Herbet, T., & Besse, M. (2018). Origin and paleoenvironmental significance of Fe Mn nodules in the Holocene perialpine sediments of Geneva basin, Western Switzerland. *Applied Clay Science*, 160, 22–39. <https://doi.org/10.1016/j.clay.2018.01.027>
- Sherwood, S. C., Simek, J. F., & Polhemus, R. R. (1995). Artifact size and spatial process: Macro- and microartifacts in a Mississippian house. *Geoarchaeology*, 10(6), 429–455. <https://doi.org/10.1002/gea.3340100603>
- Sigaut, F. (1975). *L'agriculture et le feu. Rôle et place du feu dans les techniques de préparation du champ de l'ancienne agriculture européenne*. École des Hautes Études en Sciences Sociales et Mouton & Co.
- Steensberg, A. (1993). *Fire-clearance husbandry: Traditional techniques throughout the world*. Poul Kristensen.
- Stuedel, A., Kleeberg, R., Koch, C. B., Friedrich, F., & Emmerich, K. (2016). Thermal behavior of chlorites of the clinochlore-chamosite solid solution series: Oxidation of structural iron, hydrogen release and dehydroxylation. *Applied Clay Science*, 132–133, 626–634. <https://doi.org/10.1016/j.clay.2016.08.013>
- Stoops, G., Marcelino, V., & Mees, F. (2018). *Interpretation of micro-morphological features of soils and regoliths*. Elsevier.
- Sun, Z., Jiang, Y., Wang, Q., & Owens, P. R. (2018). Fe–Mn nodules in a Southern Indiana loess with a fragipan and their soil forming significance. *Geoderma*, 313, 92–111. <https://doi.org/10.1016/j.geoderma.2017.10.025>
- Tan, W., Liu, F., Li, Y., Hu, H., & Huang, Q. (2006). Elemental composition and geochemical characteristics of iron–manganese nodules in main soils of China. *Pedosphere*, 16(1), 72–81. [https://doi.org/10.1016/s1002-0160\(06\)60028-3](https://doi.org/10.1016/s1002-0160(06)60028-3)
- Thomaz, E. L. (2017). High fire temperature changes soil aggregate stability in slash-and-burn agricultural systems. *Scientia Agricola*, 74(2), 157–162. <https://doi.org/10.1590/1678-992x-2015-0495>
- Thomaz, E. L. (2021). Effects of fire on the aggregate stability of clayey soils: A meta-analysis. *Earth-Science Reviews*, 221, 103802. <https://doi.org/10.1016/j.earscirev.2021.103802>
- Vepraskas, M. J. (2000). Morphological features of seasonally reduced soils. In J. L. Richardon, & M. J. Vepraskas (Eds.), *Wetland soils: Hydrology, landscape and classification*. Lewis Publisher. <https://doi.org/10.1201/9781420026238.ch7>
- Weiner, S. (1998). Evidence for the use of fire at Zhoukoudian, China. *Science*, 281(5374), 251–253. <https://doi.org/10.1126/science.281.5374.251>
- Xue, B., Huang, L., Huang, Y., Yin, Z., Li, X., & Lu, J. (2019). Effects of organic carbon and iron oxides on soil aggregate stability under different tillage systems in a rice–rape cropping system. *CATENA*, 177, 1–12. <https://doi.org/10.1016/j.catena.2019.01.035>
- Zavala, L., De Celis, R., & Jordán, A. (2014). How wildfires affect soil properties. A brief review. *Cuadernos de Investigación Geográfica*, 40(2), 311. <https://doi.org/10.18172/cig.2522>

SUPPORTING INFORMATION

Additional supporting information can be found online in the Supporting Information section at the end of this article.

How to cite this article: Giosa, A., Delbey, T., Menbrivès, C., Rasmussen, K. L., Elliott, M., & Petit, C. (2022). Indurated soil nodules: A vestige of ancient agricultural practices? *Geoarchaeology*, 37, 870–886. <https://doi.org/10.1002/gea.21926>

Indurated soil nodules: a vestige of ancient agricultural practices?

Giosa, Alain

2022-08-04

Attribution 4.0 International

Giosa A, Delbey T, Menbrivès C, et al., (2022) Indurated soil nodules: a vestige of ancient agricultural practices?, *Geoarchaeology*, Volume 37, Issue 6, November/December 2022, pp. 870-886

<https://doi.org/10.1002/gea.21926>

Downloaded from CERES Research Repository, Cranfield University